



# Diverse Community Structures in the Neuronal-Level Connectome of the *Drosophila* Brain

Chi-Tin Shih<sup>1,2</sup> · Yen-Jen Lin<sup>2,3</sup> · Cheng-Te Wang<sup>4</sup> · Ting-Yuan Wang<sup>5</sup> · Chih-Chen Chen<sup>1</sup> · Ta-Shun Su<sup>4</sup> · Chung-Chuang Lo<sup>3,4</sup> · Ann-Shyn Chiang<sup>3,4,5,6,7,8,9</sup>

Published online: 3 December 2019  
© Springer Science+Business Media, LLC, part of Springer Nature 2019

## Abstract

*Drosophila melanogaster* is one of the most important model animals in neurobiology owing to its manageable brain size, complex behaviour, and extensive genetic tools. However, without a comprehensive map of the brain-wide neural network, our ability to investigate brain functions at the systems level is seriously limited. In this study, we constructed a neuron-to-neuron network of the *Drosophila* brain based on the 28,573 fluorescence images of single neurons in the newly released *FlyCircuit* v1.2 (<http://www.flycircuit.tw>) database. By performing modularity and centrality analyses, we identified eight communities (right olfaction, left olfaction, olfactory core, auditory, motor, pre-motor, left vision, and right vision) in the brain-wide network. Further investigation on information exchange and structural stability revealed that the communities of different functions dominated different types of centralities, suggesting a correlation between functions and network structures. Except for the two olfaction and the motor communities, the network is characterized by overall small-worldness. A rich club (RC) structure was also found in this network, and most of the innermost RC members innervated the central complex, indicating its role in information integration. We further identified numerous loops with length smaller than seven neurons. The observation suggested unique characteristics in the information processing inside the fruit fly brain.

**Keywords** Drosophila · Neural networks · Connectome · Community · Centrality

---

Chi-Tin Shih and Yen-Jen Lin contributed equally to this work.

**Electronic supplementary material** The online version of this article (<https://doi.org/10.1007/s12021-019-09443-w>) contains supplementary material, which is available to authorized users.

- ✉ Chi-Tin Shih  
shih.chi.tin@gmail.com
- ✉ Chung-Chuang Lo  
cclo@mx.nthu.edu.tw
- ✉ Ann-Shyn Chiang  
aschiang@life.nthu.edu.tw

- <sup>1</sup> Department of Applied Physics, Tunghai University, Taichung, Taiwan
- <sup>2</sup> National Center for High-performance Computing, Hsinchu, Taiwan
- <sup>3</sup> Brain Research Center, National Tsing Hua University, Hsinchu, Taiwan

- <sup>4</sup> Institute of Systems Neuroscience, National Tsing Hua University, Hsinchu, Taiwan
- <sup>5</sup> Institute of Biotechnology and Department of Life Science, National Tsing Hua University, Hsinchu, Taiwan
- <sup>6</sup> Department of Biomedical Science and Environmental Biology, Kaohsiung Medical University, Kaohsiung, Taiwan
- <sup>7</sup> Graduate Institute of Clinical Medical Science, China Medical University, Taichung, Taiwan
- <sup>8</sup> Institute of Molecular and Genomic Medicine, National Health Research Institutes, Zhunan, Taiwan
- <sup>9</sup> Kavli Institute for Brain and Mind, University of California at San Diego, La Jolla, CA, USA

## Introduction

Connectome, the comprehensive map of neural connections in the brain, provides key information for investigating the structure and functions of the brain (Sporns et al. 2005; Lichtman et al. 2008; Pastrana 2013; Morgan and Lichtman 2013; Helmstaedter 2013; Landhuis 2017; Plaza et al. 2014). Studying connectome may accelerate our understanding and ability to find treatments for brain disorders. Indeed, to carry out this major task of science, governments and private foundations have launched several large-scale projects, including the BRAIN initiative in the United States (Jorgenson et al. 2015) and the Human Brain Project in Europe (Markram 2012). Thanks to rapid advancements in neuroimaging technologies (Levoy et al. 2006; Huisken et al. 2004; Planchon et al. 2011; Bahlmann et al. 2007; Bewersdorf et al. 1998; Lo and Chiang 2016; Denk and Horstmann 2004; Mayerich et al. 2008) and complex network analytics (Albert and Barabasi 2002; Bullmore and Sporns 2009; Sporns et al. 2011; Fornito et al. 2016) in recent years, connectomic analysis at the single-cell level has become possible.

However, despite this level of progress, studying single-cell level connectome of the human brain, which consists of  $8.6 \times 10^{10}$  neurons (Azevedo et al. 2009) with  $\sim 10^{15}$  connections, is still far beyond our capability owing to the complexity involved in image acquisition and network analysis. Therefore, current studies of brain-wide networks in human or other mammals primarily focus on connectome at the macroscopic or mesoscopic levels, namely, the connections between cortical or subcortical regions (Bota et al. 2003; Bota et al. 2015; Zingg et al. 2014; Gămănuț et al. 2018; Knox et al. 2018).

Alternatively, simpler but more manageable animals such as *Drosophila melanogaster* (fruit fly), are used as a model system for brain research at the single-neuron resolution. A fruit fly brain consists of approximately 135,000 neurons, and one of the largest databases of fruit fly brain images, the FlyCircuit database (<http://flycircuit.tw>), hosts 28,573 neuron images (Shih et al. 2015; Chiang et al. 2011). Based on the data available in FlyCircuit, we recently constructed and analysed a fruit fly brain network at the mesoscopic level (Shih et al. 2015), which carries information about links between the brain regions, or *Local Processing Units* (LPUs). LPUs are defined as the brain regions which possess their own populations of local interneurons and which deliver or receive information via bundled neural tracts to or from other regions (see the list of LPUs with their positions and full names in Shih et al. (2015)). In this previous study (Shih et al. 2015), we discovered the super-LPU functional modules, which are clusters of LPUs with dense intra-modular connections and sparse inter-modular connections. The functional role of each module was identified based on the network structure and the prior knowledge of the functions of several well-studied LPUs.

Specifically, we identified the olfactory, visual, auditory, and pre-motor modules. Moreover, a model for the information flow in the mesoscopic brain network was constructed based on the analysis. The study extended our understanding about the functions of the LPUs and super-LPU functional modules in the fruit fly brain.

In Shih et al. (2015), the analysis was conducted based on the prior knowledge of LPUs, and only the connections between LPUs at the mesoscopic level were considered. In the present study, to advance our knowledge of the architecture of the *Drosophila* brain network at an even more detailed level, we constructed a microscopic connectome of the fruit fly brain based on traced single-neuron fluorescence images together with the predicted polarity and connectivity. We asked whether the same modular structure previously observed in the LPU-to-LPU network could be verified in the neuron-to-neuron network without the information of LPUs. We further asked, whether each module exhibits a different network connectivity and architecture at the microscopic level. To this end, we conducted several complex network analyses on this neuron-to-neuron network, and performed cross-scale comparison between the results from the new analysis and those obtained from the mesoscopic LPU-to-LPU network.

We found that the microscopic neural network forms several communities, which are consistent with the functional modules previously discovered (Shih et al. 2015), and each community exhibits different structural properties in terms of centralities, small-worldness, and loops. The centralities are a collection of measures that represent the importance of a node based on its connectivity, and small-worldness indicates how well the nodes form closely interacting clusters while still maintain efficient intra-cluster communication. These measures had been widely used in analysis of brain networks (Bota et al. 2015; Bullmore and Sporns 2009; Harriger et al. 2012; Rubinov and Sporns 2010; Shih et al. 2015; Sporns et al. 2011; Sporns et al. 2005; Kaiser 2015). Loops are the structures in a brain network capable of reiterating signals or maintain persistent neural activity and are believed to be important for basic brain functions such as synchronization (Wu et al. 2011; Krashes et al. 2007; Shih et al. 2015; Mi et al. 2013; Cleland and Linster 2005; Kashiwadani et al. 1999). The structural distinctions discovered in the present study imply functional differences between the communities. Our analysis provides deep insights into the structural organisation and its functional association of the *Drosophila* brain network.

## Methods

### Data Source

The neuron-to-neuron network was constructed based on data obtained from the latest version (v1.2) of the *FlyCircuit*

database (Chiang et al. 2011; Shih et al. 2015; Huang et al. 2019), which hosts a total of 28,573 images of single neurons—a moderate increment from the previous version (v 1.1) of the database, which hosts 23,579 images (Shih et al. 2015). Among these neurons, 22,834 are from females and were used to assemble the network used in this study. Note that the previous LPU-to-LPU network analysis was based on the version 1.1 database (Shih et al. 2015), whereas the present study is based on the latest version 1.2 database. The skeleton of each neuron, including those that were in the version 1.1 database and those newly added, was traced using a combination of two algorithms (Lee et al. 2012; Peng et al. 2010; Xiao and Peng 2013), and was transformed and registered in a standard brain space.

## Network Construction

The FlyCircuit database provides detailed neuron images and accurate tracing lines (skeletons) for each neuron. However, to construct a neural network using the data, the following additional information was needed: 1) polarity, i.e. axons and dendrites, of neurons and 2) connections between neurons. We describe the methods we used to estimate the parameters associated with these properties below.

First, for every neuron in the version 1.2 database (including those already present in the old version 1.1 database), we used the “skeleton-based polarity identification for neurons” (SPIN) algorithm (Lee et al. 2014) to identify the polarity of each structural domain of the individual neurons according to their morphology. Next, we estimated whether connections existed between any two given neurons. The *FlyCircuit* database provides neuron skeletons that were transformed (or warped) and registered in a standard brain space. Based on the relative positions of the neuron skeletons in the standard brain space, we could estimate the connections between neurons using a distance criterion. We considered that two neurons formed connections when the distance between a segment of the axonal arbour from one neuron and a segment of the dendritic arbour from the other neuron is smaller than one voxel, which is approximately  $1.0 \mu\text{m}$ . We found that when two neurons formed connections, there were often multiple pairs of segments meeting the distance criterion. This observation is consistent with a recent study which discovered that a large portion of postsynaptic neurons make multiple synaptic contacts with each individual presynaptic input neuron in the *Drosophila* nervous system (Schneider-Mizell et al. 2016). To validate our method of connection estimation, we used the previously published neuron innervation dataset (Lin et al. 2013a). The dataset provided detailed innervation patterns of neurons that innervate the protocerebral bridge (PB) and associated neuropils. Of the neural images examined in the study, 442 were deposited into the FlyCircuit database. We checked the predicted (by our method) connections between

these 442 neurons and found that the true positive rate (number of correctly predicted connections / number of all true connections) is 0.40, while the false positive rate (number of incorrectly predicted connections / number of neuron pairs without connections) is 0.02. Although our method captured less than a half of the true connections, the false positive is extremely low.

Using the described procedure, we were able to construct a weighted network with 22,834 nodes (neurons) and represent it by an adjacency matrix  $A$ , with  $A_{ij}$  as the connection strength (weight) between two neurons  $i$  and  $j$ , represented by the number of segment pairs that meet the distance and polarity criterion. We found that not all nodes make two-way connections with the rest of the network; specifically, some nodes only make axonal connections and others only make dendritic connections. For network analysis, in the present study we discarded those nodes and only considered the remaining 19,902 nodes in the brain network. These nodes formed a strongly connected network, in which each node can reach all others and can be reached by all others.

## Measuring the Network

The following measurements were performed on the neuron-to-neuron network using the Brain Connectivity Toolbox (BCT) (Rubinov and Sporns 2010) in MATLAB:

**Degree:** Number of connections of each node.  $D_i^{\text{out}} = \sum_{j \neq i} B_{ij}$ ,  $D_i^{\text{in}} = \sum_{j \neq i} B_{ji}$ , and  $D_i^{\text{total}} = D_i^{\text{out}} + D_i^{\text{in}}$ .  $D_i^{\text{out}}$ , and  $D_i^{\text{in}}$  are the outgoing, incoming, and total degrees for the  $i$ -th node in the network, where  $B$  is the binarized matrix of  $A$ .

**Strength:** Total weight of the connections of each node.  $s_i^{\text{out}} = \sum_{j \neq i} A_{ij}$ ,  $s_i^{\text{in}} = \sum_{j \neq i} A_{ji}$ ,  $s_i^{\text{total}} = s_i^{\text{out}} + s_i^{\text{in}}$ .  $s_i^{\text{out}}$ ,  $s_i^{\text{in}}$ , and  $s_i^{\text{total}}$  are the outgoing, incoming, and total strengths for the  $i$ -th node in the network.

**Betweenness:** For a directed and weighted network, the distance from node  $u$  to node  $v$  is defined as  $1/A_{uv}$ . The shortest paths between any two nodes are first calculated, and then the betweenness  $b_i$  is given by  $b_i = \sum_{k \neq i, j; i \neq j} \frac{\sigma_{jk}(i)}{\sigma_{jk}}$ , where  $\sigma_{jk}$  is the number of shortest paths between nodes  $j$  and  $k$ , and  $\sigma_{jk}(i)$  is the number of such paths that pass node  $i$ . The betweenness was calculated using the algorithm developed by Brandes (Brandes 2001).

**Vulnerability:** Removing a node from a network usually decreases the efficiency of information flow. Vulnerability of a node is defined as the decrease in the global efficiency (averaged inverse shortest path lengths between node pairs) of the network owing to deletion of that node (Kaiser and Hilgetag 2004).

**Dynamical importance:** The largest eigenvalue and the corresponding eigenvector of the adjacency matrix of the

network are known to affect many dynamical properties of the network. Suppose the removal of node  $i$  changes the largest eigenvalue of the matrix from  $\lambda$  to  $\lambda_i$ , the dynamical importance  $I_i$  of node  $i$  is thus defined as  $I_i = \frac{-(\lambda_i - \lambda)}{\lambda}$ .

**Closeness:** Closeness is defined as the averaged inverse distance of the shortest paths between a node and all other nodes. Incoming and outgoing closeness for node  $i$  are,  $c_i^{in} = \frac{1}{N-1} \sum_{j \neq i} \frac{1}{d_{ji}}$ ,  $c_i^{out} = \frac{1}{N-1} \sum_{j \neq i} \frac{1}{d_{ij}}$ , respectively. The overall closeness is  $c_i = \frac{c_i^{in} + c_i^{out}}{2}$ .

**PageRank:** Google uses this centrality to estimate the importance of web pages. The pagerank of a node measures weighted pagerank of incoming connections, which provided information of the importance of the upstream nodes. The basic idea is that a neuron collecting information from other important (high pagerank) neurons is also important. The PageRank  $PR(i)$  of node  $i$  is defined as  $PR(i) = \frac{1-d}{N} + d \sum_j \frac{PR(j)A_{ji}}{s_j^{out}}$ , where the damping factor  $d = 0.85$  (Brin and Page 1998). This value is commonly used in literature and the choice of  $d$  value has only a minor impact to the relative rank of the nodes.

**Community detection and modularity:** The community structure is represented by the partition vector  $C = (c_1, c_2, \dots, c_N)$ , where  $c_i$  is the community to which node  $i$  belongs. The best community structure of a network is determined by finding the partition  $C$  with the maximal modularity  $Q$ , defined as

$$Q = \frac{1}{m} \sum_{ij} \left( A_{ij} - \frac{s_i^{out} s_j^{in}}{2m} \right) \delta(c_i, c_j) \quad (\text{Newman 2006}), \text{ where } m = \sum_{ij} A_{ij}, \delta(c_i, c_j) = 1 \text{ if } c_i = c_j \text{ and } = 0 \text{ otherwise.}$$

**Within-community strength.** The within-community strength  $z_i$  is defined by  $z_i = \frac{\kappa_i - \bar{\kappa}_{c_i}}{\sigma_{\kappa_{c_i}}}$ , where  $\kappa_i$  is the summation of the edge strength of node  $i$  to neighboring nodes in the same community,  $c_i$ .  $\bar{\kappa}_{c_i}$  and  $\sigma_{\kappa_{c_i}}$  are the average and standard deviation of  $\kappa$  for all the nodes in community  $c_i$  (Guimera and Amaral 2005).

**Participation coefficient.** The participation coefficient  $P_i$  is defined by  $P_i = 1 - \sum_{c=1}^{N_c} \left( \frac{\kappa_{ic}}{s_i} \right)^2$ .  $\kappa_{ic}$  is the summation of the edge strength of node  $i$  connecting to other nodes in community  $c$ .  $s_i$  is the total strength of node  $i$ .  $P_i$  ranges from zero to one. A connector node whose strength is evenly distributed among all the communities will have a large (close to one)  $P_i$  (Guimera and Amaral 2005). On the other hand,  $P_i = 0$  for a node that is entirely local to a community and does not make connections with other communities.

**Small-world index** The small-world index (SWI) is defined as  $SWI = \frac{(\gamma/\bar{\gamma})}{(p/\bar{p})}$ , where  $\gamma$  is the averaged clustering coefficient (Fagiolo 2007) of all nodes and  $p$  is the averaged shortest path

lengths of all node pairs  $p$ .  $\bar{\gamma}$  and  $\bar{p}$  are the ensemble averages for 1000 realisations of the randomised networks.  $SWI > 1$  indicates the characteristics of the small world.

**Loops** Loops are special types of motifs and are characterized by a set of serially connected nodes with the last node connected back to the first one (Milo et al. 2002). In a directed and weighted network, we define a loop  $L$  with length  $\ell$  as a set of serially connected nodes represented by

$$L = \{n_1, n_2, \dots, n_\ell; A(n_1, n_2), A(n_2, n_3), \dots, A(n_i, n_{i+1}), \dots, A(n_{\ell-1}, n_\ell), A(n_\ell, n_1)\}$$

where  $n_i$  is the  $i$ -th node and  $A(n_i, n_j)$  is the connection strength between nodes  $n_i$  and  $n_j$ . The strength of a loop is defined as the weakest connection in  $L$ :  $S_L = \min(A(n_1, n_2), A(n_2, n_3), \dots, A(n_i, n_{i+1}), \dots, A(n_{\ell-1}, n_\ell), A(n_\ell, n_1))$ .

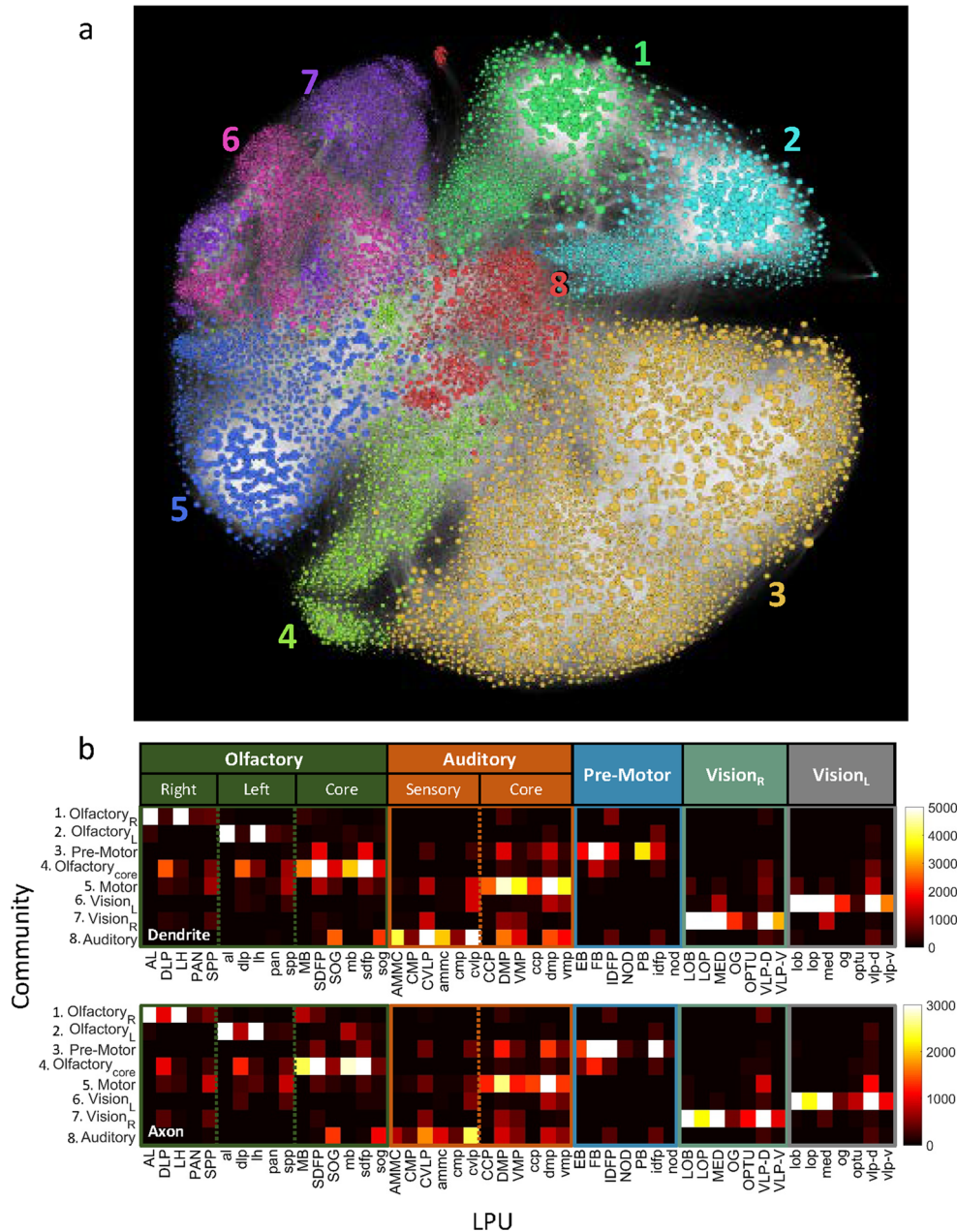
The computation for searching long loops in a large network is very time-consuming. To overcome this computational barrier, we removed the connections that are weaker than a threshold and the network was separated into many smaller sub-networks. To identify a loop, we started from a node and searched its downstream links. We repeated this procedure until we grew all the self-avoiding chains from the starting neuron with length  $\ell - 1$ . A loop could be identified if there was a link from the end of a chain to the starting neuron. Finally, the existence of shortcuts in each loop was checked to determine the irreducibility of the loop.

## Results

### Community Structure

We first studied the community structure of the network. A network forms communities if its nodes can be divided into several groups, with the intra-group connections significantly denser than the inter-group connections. Each of these groups of nodes is called a community in the network. We identified the community in the neuron-to-neuron *Drosophila* brain network based on the algorithm proposed by Newman (Newman 2006), and found that the network could be divided into eight communities (Fig. 1a). Numbers of neurons in each community are listed in Table 1. Note that the communities were identified without the information of LPUs. However, in order to assess the putative functions of these communities, we analysed the LPUs innervated by the dendrites and axons of the neurons in each community (Fig. 1b). Intriguingly, we found that this community structure was highly consistent with the structure and organisation of the functional modules and their submodules (indicated by the coloured frames in Fig. 1b) in the previously described LPU-to-LPU mesoscopic network (Shih et al. 2015). Neurons belonging to the same

**Fig. 1 Community structure of the *Drosophila* brain.** **a** Neuron-to-neuron network of the *Drosophila* brain. Each dot is a node representing one neuron in the network. The size of each dot is proportional to the degree of the neuron. We divided the neuron-to-neuron network of the *Drosophila* into eight communities by maximizing modularity (see Methods). **b** The community-function association can be inferred by inspecting how the dendrites (upper panel) and axons (lower panel) of neurons in each community innervate the LPUs. The ordinate represents communities 1–8 (from top to bottom), while the abscissa represents the 49 LPUs that are grouped by their functional modules indicated by the coloured frames, as described in Shih et al. (Shih et al. 2015). The colour in each cell indicates the total number of dendritic (upper panel) and axonal (lower panel) terminal points in each LPU from all neurons of each community. The clear segregation of innervated LPU modules between communities implies their functions: 1 → right olfactory, 2 → left olfactory, 3 → pre-motor, 4 → olfactory core, 5 → motor, 6 → left visual, 7 → right visual, and 8 → auditory sensory (see Table S1)



community innervated primarily the LPUs of the same functional module. In addition, the distribution for dendritic and axonal terminals for each community was highly symmetric across the hemispheres. To avoid ambiguity, we use the term “functional modules” for the sets of LPUs clustered from the LPU-to-LPU network in the previous study (Table S1 in (Shih et al. 2015)), and the term “communities” for the sets of neurons clustered from the neuron-to-neuron network in the present study.

For all neurons in each community, by counting the numbers of dendritic/axonal terminal points located in each of the 49 LPUs (Fig. 1b, the upper and lower panels are for dendritic and axonal terminal points, respectively), we found that

communities 1 and 2 corresponded to the right and left olfaction, respectively. Furthermore, the majority of the neurons in the two communities innervated two LPUs: AL, the target of the olfactory sensory neuron projections, and LH, one of the downstream regions of AL. This observation implies that the two communities are the early and sensory part of the olfactory system. These two communities also formed connections with the ipsilateral VLP-D, IDFP, and DMP. Neurons in community 3 mostly innervated the central complex (CX), or the pre-motor centre (Fig. 1b). This community also made connections with the bilateral DMP and SDFP, which were identified as rich club (motor centre) members of the LPU-to-LPU network. Community 4 linked the bilateral olfactory cores,

**Table 1** Small-world properties of the communities in the neuron-to-neuron network. All communities, except for the right olfactory, left olfactory, and motor, are small worlds

Network/Subnetwork	Number of neurons	Connection density	Clustering coefficient	Path length	Small-world index
Whole Brain	19,902	0.9%	4.35(1)	1.39(1)	3.13(1)
Olfactory, right	1247	12.8%	2.25(2)	3.86(2)	0.58(1)
Olfactory, left	1184	14.5%	2.59(2)	6.47(4)	0.40(1)
Pre-Motor	3637	7.7%	2.92(1)	0.969(2)	3.01(2)
Olfactory, core	2991	3.3%	3.17(2)	1.41(1)	2.25(3)
Motor	1262	14.5%	1.62(1)	1.88(0)	0.86(1)
Visual, left	3965	1.9%	2.97(1)	1.10(1)	2.70(3)
Visual, right	4028	1.9%	3.20(2)	1.07(1)	2.98(4)
Auditory	1588	6.0%	3.95(4)	1.00(1)	3.94(6)

and exchanged information with the central complex (Fig. 1b). Community 5 mainly connected the LPUs in the motor centre with the major components located in the core of the auditory module (DMP, CCP, and VMP) (Fig. 1b). VLP-D (visual), CVLP (auditory sensory), and SDFP (olfactory core) were also included in this community. Neurons in communities 6 and 7 innervated the LPUs of the visual modules of the left and right hemispheres, and they also connected the auditory core (Fig. 1b). Finally, community 8 was centred on the sensory part (mainly AMMC and CVLP) of the auditory module (Fig. 1b). The innervation to the auditory core was also strong. Notably, this community made P a strong connection with SOG, a putative output LPU from the brain to the body.

In summary, our results suggest that the communities 1, 2, and communities 6, 7 are specialised for the olfactory and visual senses, respectively. Community 8 is for the auditory sense, but also strongly couples with the motor centre and the putative output gateway SOG. The direct connection between sensory input and motor output suggests that this community could be related to the function of fast reaction to external stimuli. Communities 3, 4, and 5 may carry out more complex functions which require direct communication between the sensory, pre-motor, and motor modules. Based on the analysis, in the following sections of this paper, we refer to communities 1–8 as right olfactory, left olfactory, pre-motor, olfactory core, motor, left visual, right visual, and auditory, respectively.

## Hub and Connector

Next, we analysed the network structure of each community by investigating how each neuron makes connections across communities and within the community to which it belongs. To this end, we calculated within-community strength  $Z_i$  and participation coefficient  $P_i$  for each neuron  $i$  according to Guimera and Amaral (2005) and plotted the scatter plots of  $Z_i$  and  $P_i$  for each community (Fig. 2). Guimera and Amaral (2005) defined node types based on the  $Z$  and  $P$  values. A

node  $i$  is called a “hub” of its own community if  $Z_i \geq 2.5$ , or called a “connector” if  $P_i > 0.62$ . Seven types of nodes were further defined: ultra-peripheral R1 ( $Z_i < 2.5$ ,  $P_i \leq 0.05$ ); peripheral R2 ( $Z_i < 2.5$ ,  $0.05 < P_i \leq 0.62$ ); non-hub connectors R3 ( $Z_i < 2.5$ ,  $0.62 < P_i \leq 0.8$ ); non-hub kinless R4 ( $Z_i < 2.5$ ,  $0.8 < P_i \leq 1$ ); provincial hubs R5 ( $Z_i \geq 2.5$ ,  $P_i \leq 0.3$ ); connector hubs R6 ( $Z_i \geq 2.5$ ,  $0.3 < P_i \leq 0.75$ ); and kinless hubs R7 ( $Z_i \geq 2.5$ ,  $0.75 < P_i \leq 1$ ) (Guimera and Amaral 2005).

Close inspection of the  $Z_i$  and  $P_i$  plots (Fig. 2) revealed that the eight communities could be roughly classified into three groups based on the types of hubs within each community. The first group comprised the two olfactory sensory communities, which contained only highly localised provincial hubs R5 ( $P_i \sim 0.1$ ). Most neurons which made stronger connections with other communities ( $P_i > 0.3$ ) in these two communities were non-hub. The result implies that the roles of the community centre (hub) and gateway to other communities are played by distinct neurons in the olfactory sensory system. Such disassociation of community centres can be explained by the large number of local neurons densely packed into the antennal lobes. These local neurons were only and heavily connected with other neurons in the antennal lobes, while the inter-community projections were carried out by the project neurons in the same LPUs.

The second group was formed by the two visual communities, which possessed many more connector hub neurons (R6) than the olfactory sensory system (group 1) did. Because of the large  $Z$  and  $P$  values, these connector hub neurons in the visual system played both the roles of a community centre and a gateway.

The third group consisted of the three central brain communities (olfactory core, pre-motor, and motor) and the auditory community. Their  $Z$  and  $P$  distributions were between those of the first two groups. Specifically, a few connector hubs were observed, and the distribution of  $Z_i$  for  $P_i > 0.3$  was much broader than the olfactory sensory system (group 1).

Note that the precise boundary values of  $Z_i$  and  $P_i$  for node-type classification are not important for the purpose of our

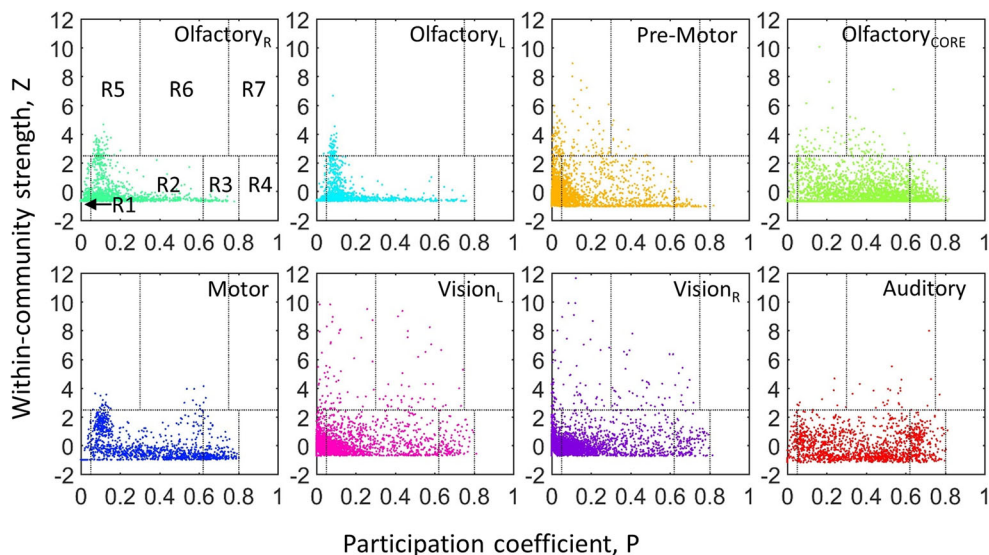


**Fig. 2** Within-community strength (Z) and participation coefficient (P) of neurons in each community. Each dot on the plot indicates the Z and P values of one neuron, and each panel represents one community. The Z-P scatter plot can be divided into seven regions: R1 (ultra-peripheral), R2 (peripheral), R3 (non-hub connector), R4 (non-hub kinless), R5 (provincial hub), R6 (connector hub), and R7 (kinless hub). Based on the

distribution of hub neurons (R5-R7), the eight communities can be classified into three groups. Group 1 (Olfactory<sub>L,R</sub>) only contains highly localised provincial hub neurons (R5). Group 2 (Vision<sub>L,R</sub>) contains many more connector hub neurons (R6) than group 1. For group 3 (the reset), the distributions of hub types fall between those of groups 1 and 2

analysis as we compared different modules only based on the relative distribution of the nodes, not their exact numbers, in different domains.

### Centrality of the Neurons

In addition to the community-based measures, such as within-community strength and participation coefficient, we also investigated the network structure using community-independent measures, which better reflected the global properties of the network, as many neurons make connections across communities. We first analysed several types of centralities (Rubinov and Sporns 2010; Shih et al. 2015) (see Methods for detail) of the *Drosophila* brain network. Interestingly, neurons with the highest number of centralities of different types located in different communities. Neurons with the top 10 degree (Fig. S1a), strength (Fig. S1b), betweenness (Fig. S1c), closeness centralities, and dynamical importance belonged to the pre-motor, olfactory, visual (left and right), motor, and olfactory (left and right) communities, respectively. Neurons with the highest vulnerability and PageRank were diversely distributed in several communities. Fig. S2 displays the neurons with the top 10 dynamical importance (panels a1–a10), vulnerability (panels b1–b10), closeness (panels c1–c10), and PageRank (panels d1–d10) centralities of the network. We further calculated the global centrality of each neuron according to the rankings of all seven types of centralities. The top 10 neurons with highest global centrality are displayed in Fig. S3.

Next, we analysed the distribution of neurons with high centralities across the communities (Figs. 3 and S4). Neurons in the pre-motor and olfactory communities dominated the degree and strength centralities, respectively (Fig. 3a and b). The betweenness centrality was more evenly distributed across communities, except for that of the left vision community, which had several neurons with very large betweenness ( $>10^{-2}$ ) (Fig. 3c). Neurons in the motor community had larger closeness (Fig. S4a) and olfactory sensory communities dominated the dynamical importance (Fig. S4c). The distributions of PageRank (Fig. S4b) and vulnerability (Fig. S4d) were similar between the eight communities. On calculating the total global centrality score for each community, we found that the pre-motor and motor communities had the largest scores (Fig. 3d).

### Degree and Strength Distributions

We have demonstrated the diversity in terms of connectivity and centrality across communities. Moreover, diversity can also be observed at the single-neuron level. We plotted the distributions of degree (Fig. 4a) and strength (total weight of the connections of each node) for the neurons in the brain network (Fig. 4b) and found that both exhibited a fat tail, indicating broadly distributed degree and strength. Specifically, the degree distribution decayed exponentially (for degree less than 2000), while the strength distribution exhibited a power law-like tail. It was interesting to further investigate whether the strength of a connection correlated

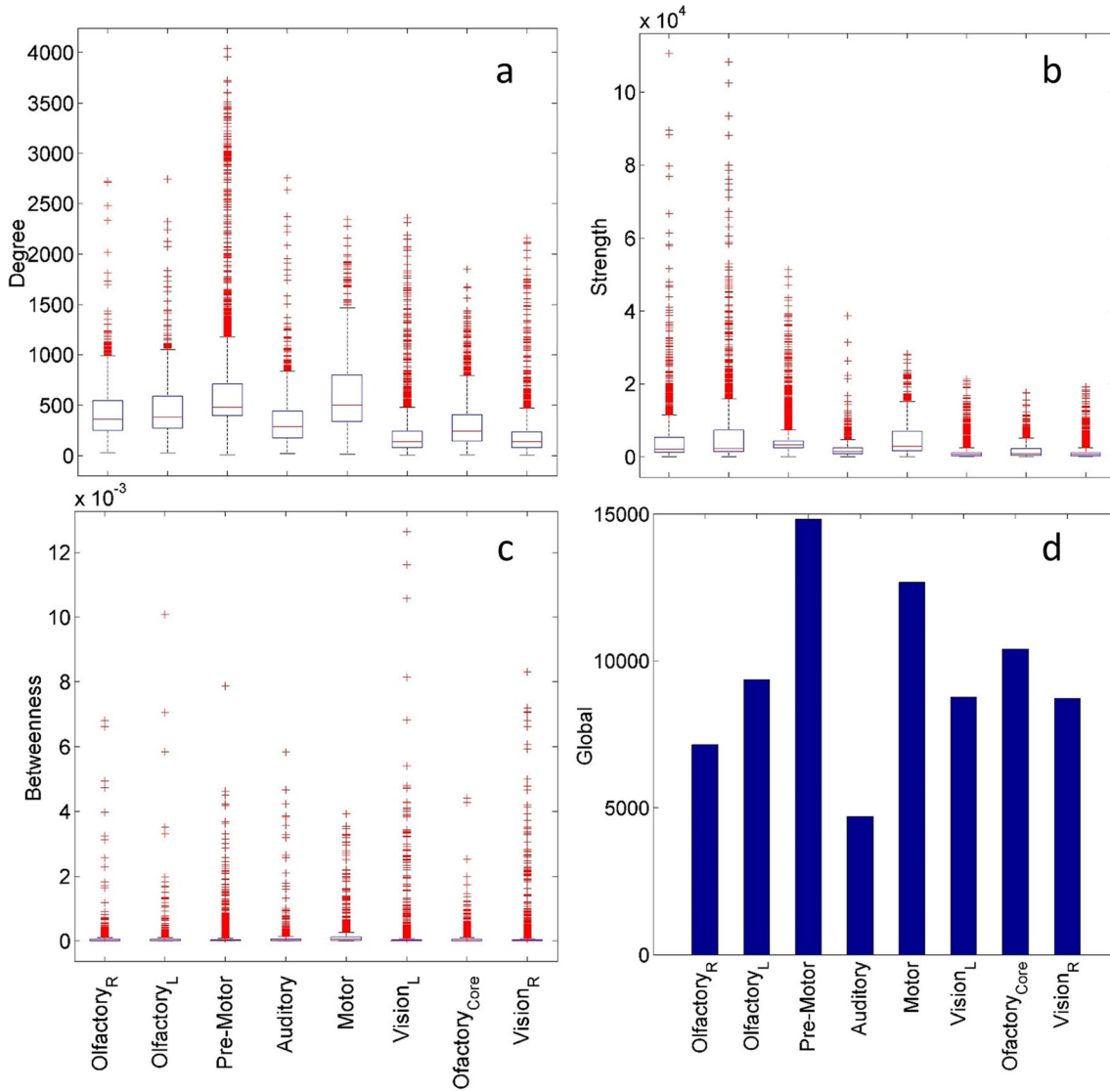


**Fig. 3 Statistics of the centralities for the eight communities.** The box plots for the distribution of **a** degree, **b** strength, and **c** betweenness centralities for neurons in the eight communities. The top and bottom ends of the whiskers indicate the highest datum within 1.5 interquartile range (IQR) of the upper quartile and the lowest datum within 1.5 IQR of the lower quartile, respectively. Degree and strength centralities are

dominated by the pre-motor and olfactory neurons, respectively. Although not so clear-cut as in the degree and strength centralities, most of the neurons with top betweenness centrality belong to the visual communities. **d** Total global centrality for each of the eight communities. Pre-motor and motor neurons have the largest values

with the degrees of associated neurons. If such a correlation did not exist, the averaged strength of the nodes with degree  $k$  would simply be  $k$  multiplied by the average weight of the edges in this network, and the two distributions would have identical behaviour (Barrat et al. 2004). We plotted a scatter plot of the strength and degree of each neuron (inset of Fig. 4a) and found surprising distributions, in which the neurons were segregated into two branches on the plot. The strengths of the neurons in the lower branch were roughly proportional to the degrees, whereas the strengths of the neurons in the upper branches (mainly the olfactory neurons in communities 1 and 2) grew much faster with the degree. These high-strength neurons gave rise to the fat tail of the strength

distribution in Fig. 4b. Furthermore, points in the lower branch in the inset of Fig. 4a are roughly clustered by colours (representing their communities), implying that the degree and strength distribution are distinct in different communities.

We further investigated the within-community degree and strength for neurons in each community by removing inter-community connections (Fig. S5). We found that although the degree and strength distributions for most communities exhibited exponential and power-law tails, respectively, there were some exceptions. The degree distributions of the pre-motor and motor communities were bimodal, while the auditory community exhibited a single peak without a fat tail. The strength distribution of the motor community was bimodal

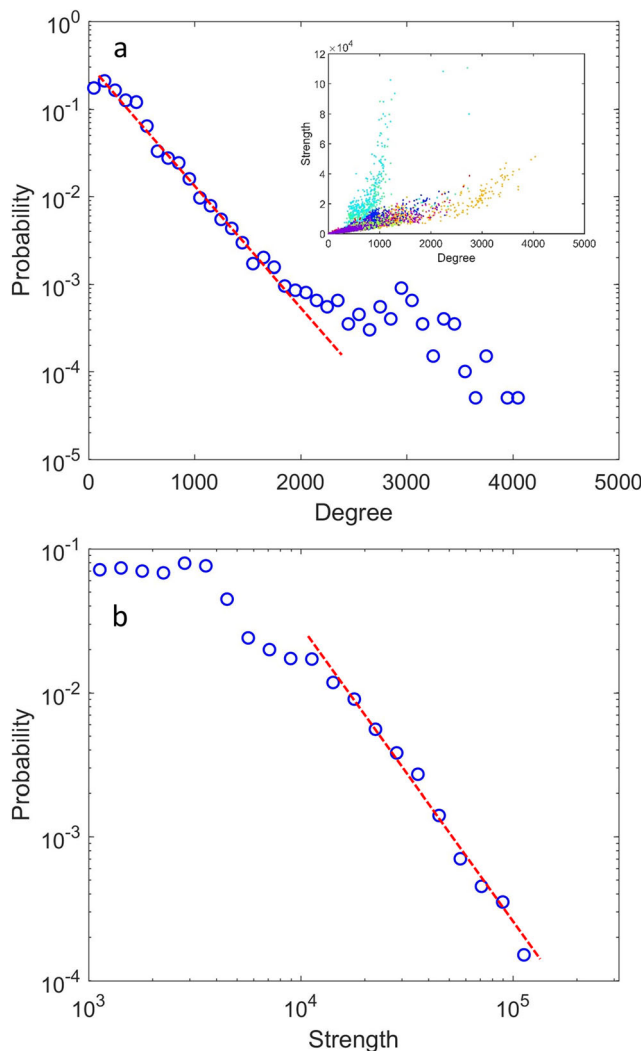


**Fig. 4** Degree and strength of distribution of the network. At the neuronal level, the distributions of (a) degree and (b) strength exhibit an exponential and a power-law decay tail, respectively. Inset: Scatter plot of the degree and strength for each neuron. Each dot is colour-coded by its community, as in Fig. 1a

and the olfactory core community exhibited a power-law tail with different exponents in the small versus large strengths.

## Rich Club

The microscopic brain network also contained rich clubs (RCs) (Harriger et al. 2012) as previously observed in the mesoscopic network (Shih et al. 2015). The innermost rich club ( $RC_i$ ) had five member neurons, which were all located in the pre-motor community. The six members of another RC with the smallest  $p$  value ( $RC_p$ ) were also all pre-motor neurons (Fig. S6). Ten of these 11  $RC_i$  and  $RC_p$  members were driven by the tyrosine hydroxylase (TH)-GAL4 driver; hence, they were putative dopaminergic neurons.

The pre-motor centre plays a pivotal role in the brain functions by integrating the sensory input and sending signals to

the motor centre for action (Shih et al. 2015; C. Y. Lin et al. 2013a; Wessnitzer and Webb 2006; Homberg 2008; Triphan et al. 2010). Thus, it is not surprising that the pre-motors neurons perform multiple functions in the network. We found that they connected to a large number of neurons (large degree), and connected to each other heavily (forming RC). Further, they were also important in information communication. For example, TH-F-20047, TH-F-30046 (both were  $RC_i$  members), and TH-F-200122 ( $RC_p$  member) were also the neurons with the fifth, eighth, and tenth largest vulnerability centralities, respectively.

## Small Worldness

Numerous studies have demonstrated small-world properties (Watts and Strogatz 1998) in several natural and social networks (Watts 1999; Newman 2010). Previous studies showed that many brain networks are also small worlds (Bassett and Bullmore 2006; Bullmore and Sporns 2009), including the mesoscopic network of the *Drosophila* brain (Shih et al. 2015). A small-world network is defined as a network with a “small-world index” (SWI, which is defined as the normalised clustering coefficient divided by the normalised path length) greater than one (Bassett and Bullmore 2006).

We calculated the SWIs of the full microscopic *Drosophila* brain network and its eight communities (Table 1), and found that, similar to the mesoscopic *Drosophila* brain network and the brain networks of other species, the full microscopic network could be characterised as a small world. We further calculated the SWIs of each community by removing the inter-community connections. Interestingly, the small-world properties were diverse across these communities: the SWIs of five communities were relatively large, whereas the other three communities—olfactory (left and right) and motor—had very small SWIs. While the small SWIs of the two olfactory communities were due to the large values of the shortest path lengths (denominator), the small SWI of the motor community was caused by its small clustering coefficient (numerator). Apart from these differences, the three non-small-world communities had two features in common: smallest number of neurons and largest intra-community connection density.

## Abundant Loops in the Brain Network

Closed loops, or recurrent connections, affect the pathways and efficiency of the information flow in neural networks (Lin et al. 2014). In the mesoscopic *Drosophila* brain network, strong loops were found in the central brain, which may be associated with re-iteration of information integration and decision-making for complex behaviours (Shih et al. 2015).

For a weighted network, a loop is said to be “irreducible” if there is no “shortcuts” (connections between non-neighbouring nodes in the loop) with a connection stronger

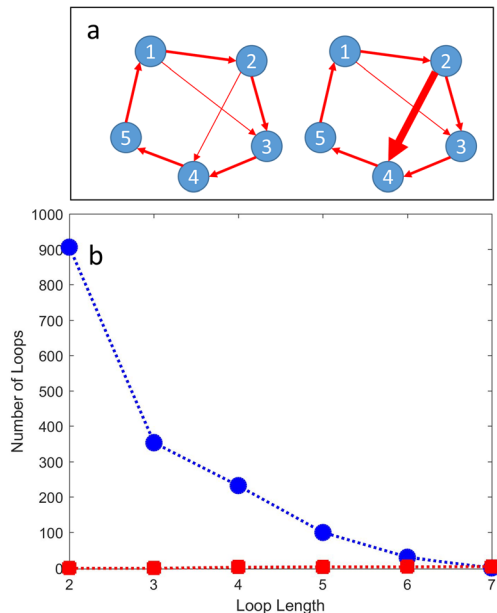


**Fig. 5** Number of irreducible loops of different lengths. **a** Schematics of irreducible loops. Left: The 5-node loop is an irreducible loop because the connections  $2 \rightarrow 4$  and  $1 \rightarrow 3$  have weaker strengths than those on the loop. In other words, there is no shortcut in the loop. Right: The 5-node loop is regarded as reducible because a shortcut exists from node 2 to 4. In this case, nodes 1–2–4–5 forms a 4-node irreducible loop. **b** The number of irreducible loops in the brain network (blue circles) is much larger than that of the random networks (red squares, averaged from 1000 realizations, error bars smaller than the symbol size) when the loop length is less than seven

than  $S_L$ . Examples for an irreducible and a reducible loop are presented in Fig. 5a. Both networks have the same connection pattern, but the irreducible loop lengths are five and four for the networks on the left and right, respectively.

We counted the number of irreducible loops with strength greater than 100 in the brain network (blue) and compared the result with those averaged from 1000 randomised networks. The distributions of incoming degree, outgoing degree, and outgoing strength were preserved in the randomisation. We discovered a significantly greater number of loops with length smaller than seven in the brain network than in the randomised networks. There was no loop with length seven or greater in either network. Four examples of irreducible 5-neuron loops are shown in Fig. S7. We found that many loops were localised in the antennal lobes, which are part of the olfactory sensory communities (Fig. S7a, b). This result is expected because the local neurons in the antennal lobes feature co-localized axons and dendrites, and therefore tend to form loops with each other or with other projection neurons. However, we also observed some long-range loops connecting other communities (Figs. S7c, d).

To further understand the properties of these loops and their functional significance, we asked how they distributed across the brain. We first investigated the intra-community loops (all nodes of the loop in the same community) with loop strength

greater than 50 and length from three to six (Fig. S8). Intriguingly, although most of the short loops  $\ell=3$  located in the olfactory communities, longer loops ( $\ell=4, 5, 6$ ) were dominated by the motor community.

Next, we investigated the distribution of the inter-community loops in the brain. To this end, we plotted the distributions of neurons which participated in an inter-community loop while connecting more than one communities (Fig. S9). For  $\ell=3$ , the contributions of the communities were roughly equal, except the auditory community. For longer loops, the olfactory communities contributed most on the inter-community loops.

## Discussion

In this study, we analysed the network structure of the directed and weighted neuron-to-neuron microscopic network of the *Drosophila* brain. In general, the observed features, such as the existence of rich clubs, modularity, small-worldness, and broad degree distributions are consistent with those found in the mesoscopic brain networks in mammalian brains (Bota et al. 2015; Bullmore and Sporns 2009; Harriger et al. 2012; Rubinov and Sporns 2010; Shih et al. 2015; Sporns et al. 2011; Sporns et al. 2005; Kaiser 2015) and in the *Drosophila* brain (Shih et al. 2015). However, the present study provides more detailed information and deeper insights into the brain network than these studies do in three ways.

First and most intriguingly, our community analysis reveals that the neurons in the microscopic network do not cluster into the neuropils or LPUs, which are the most prominent anatomical structures, mainly composed of synapses with tangled dendritic and axonal arbours. We argue that this is because the majority of the neurons are projection neurons, which connect two or more LPUs to form the functional modules. Interestingly, analyses of tract connections in the rat, cat and macaque monkey brains also revealed 4–5 modules that distribute across brain regions (Bota et al. 2015; Harriger et al. 2012; Scannell et al. 1995). Our finding implies that, in addition to the intra-LPU connections, one should also put as much as, if not more, focus on the inter-LPU connections when studying functions of the *Drosophila* brain. Indeed, a recent theoretical study suggested that spatial orientation is regulated through the interaction between two LPUs, the protocerebral bridge, and the ellipsoid body (Su et al. 2017). Moreover, without taking into account the LPUs, our analysis still reveals a community structure that is consistent with the functional modules previously discovered in the LPU-based mesoscopic network. These communities are closely related to the structures for the major brain functions, including sensory input, information integration, and action output. The result suggests that the neuron-to-neuron microscopic network carries more information about the organization of brain

functions than the information about the anatomical structures of the brain.

Second, despite the overall small-worldness observed in the microscopic *Drosophila* brain network, as in many other brain networks, our analysis further reveals diverse internal network structures in different communities. Such information is not available in the previous analysis of LPU-to-LPU brain network. Perhaps most interestingly, we found that small-worldness is not a common feature of all communities. The most heavily connected olfactory and auditory core/motor centres are in fact not small worlds. Indeed, whether small-worldness is a common property of all neural networks is still debated (Hilgetag and Goulas 2016; Muller et al. 2014). The diversity of small-worldness in the fly brain network may reflect different functional requirements in different communities. For example, the antennal lobes consist of a large number of glomeruli, with each glomerulus containing several projection neurons, which project to the downstream mushroom body and/or lateral horn with very few feedback projections (Stocker 1994; Jefferis et al. 2001). This feedforward and channel-like circuit organisation may increase the shortest path length, and hence contribute to the small SWI.

Third, the centrality measurements and rich club structure also reveal the diverse roles of neurons in each community in the network. By examining the distribution of neurons with highest centralities, we conclude the following:

1. There is a tendency for neurons in the pre-motor community to connect greater numbers of neurons and to form rich clubs. Interestingly, the community also possesses neurons with large global centrality, supporting the notion of sensorimotor integration in the central complex, a major structure in this community. Most of the top rich club neurons are putative dopaminergic neurons, implying that they may play critical roles in the pre-motor module (mainly the central complex) by modulating a large number of neurons.
2. In contrast, the olfactory neurons may not make connections with a large number of neurons. But when they make connections with one neuron, the connections tend to be strong because of the densely distributed processes of the neurons in the antennal lobes. Therefore, these neurons dominate the measure of strength centrality and dynamical importance.
3. High closeness indicates the overall short path lengths between a neuron and all other neurons. Therefore, the highest mean closeness of the motor community is presumably due to the need of other communities to initiate rapid motor responses to sensory inputs.

Considering that the neurons with the highest centralities are critically important in the structural network of the brain,

the roles of these neurons in the brain functions merit further experimental study.

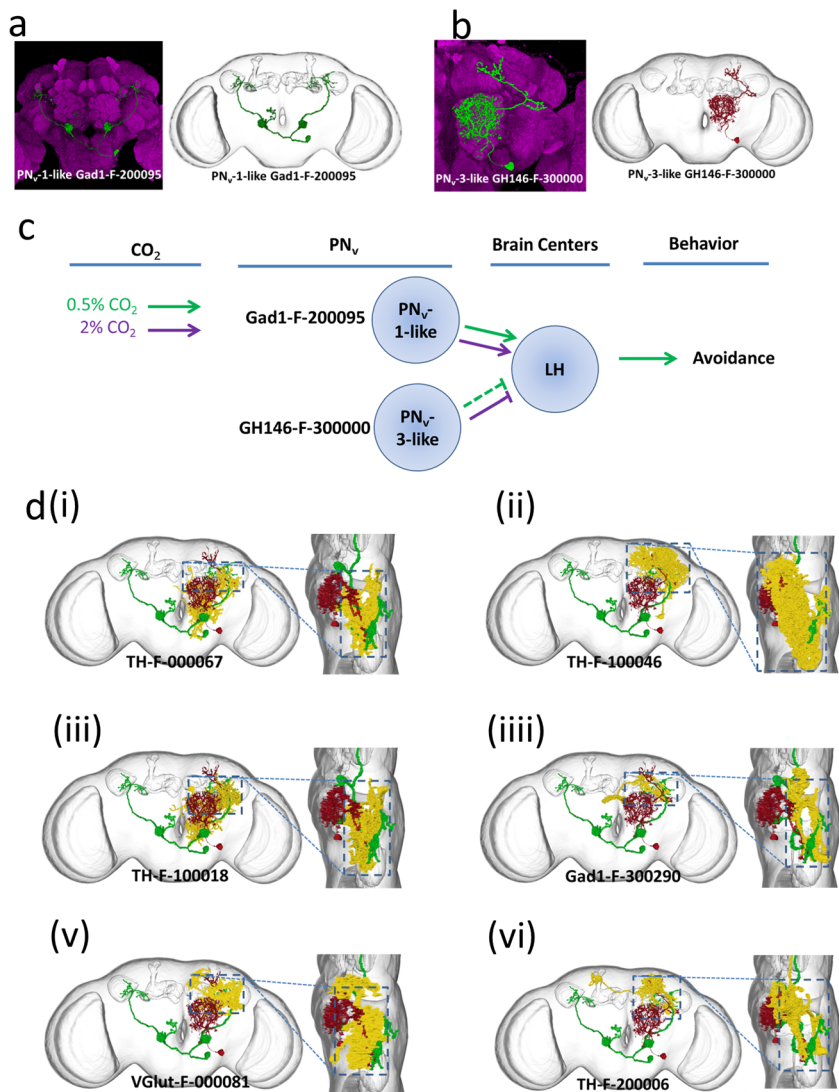
Here, we provide an example to demonstrate that how our analyses, in combination with the past experimental data and the network connectivity, can lead to novel ideas for future experiments. In a previous study, “shunting” between pathways responsible for CO<sub>2</sub> avoidance behaviour at different concentrations was observed in *Drosophila* (H. H. Lin et al. 2013b). The pathway for 0.5% CO<sub>2</sub> avoidance involved two types of projection neurons, PN<sub>v</sub>-1-like and PN<sub>v</sub>-3-like, which projected from the V glomerulus in the antennal lobe to the lateral horn. To further examine the circuit for CO<sub>2</sub> avoidance, we need to identify the common downstream neurons to PN<sub>v</sub>-1-like and PN<sub>v</sub>-3-like. From the network constructed in the present work, we found 49 putative downstream neurons of PN<sub>v</sub>-1-like and PN<sub>v</sub>-3-like. However, it is impractical to perform the complete experimental procedures including genetic engineering, functional imaging, and behavioural test on all 49 neurons, owing to the limitation of time and resources.

As avoiding CO<sub>2</sub> is an important ability for fruit flies to keep away from their predators, we conjecture that neurons involving this behaviour will occupy dominant positions in the network. According to the connectivity strength of the 49 candidate neurons with PN<sub>v</sub>-1-like and PN<sub>v</sub>-3-like, together with the global centrality measured in the present study, we reduce the list of candidates to six neurons: TH-F-000067, TH-F-100046, TH-F-100018, Gad1-F-300290, VGlut-F-000081, and TH-F-200006 (Fig. 6). They are heavily connected with PN<sub>v</sub>-1-like and PN<sub>v</sub>-3-like, and their global centrality rankings are in the top six. We expect these selected neurons to have a higher probability of being the right neurons we are looking for in the CO<sub>2</sub> avoiding circuit. This conjecture should be further validated by experiments.

We note that some of the large local neurons in the antennal lobe scored highly in various centrality measures (Figs. S1b3, S1b5-b8, S1b10, and S2a1-a10 for instance). This might look surprising and undesirable as local neurons are traditionally viewed as local modulators. However, by covering the entire antennal lobe, the large local neurons are capable of altering every olfactory signal, and therefore produce profound behavioural effects. Indeed, these local neurons may play the role of gain modulation (Olsen and Wilson 2008), which prevents the projection neurons from overloading under strong odour inputs. Removing these neurons could significantly alter the response of the olfactory system to every odour. Hence, our findings of the high centralities of local neurons in the network may provide a novel picture about their roles in brain dynamics.

Our finding of the distinct forms of the degree (exponential) and strength (power law) distributions of the neurons in the network suggests the need to build a new network growth model. However, this is beyond the scope of this paper and will be discussed elsewhere.

**Fig. 6 Prediction of the downstream neurons in the CO<sub>2</sub> avoiding circuit. a** A typical PN<sub>v</sub>-1-like (Gad1-F-200095) neuron. **b** A typical PN<sub>v</sub>-3-like (GH146-F-300000) neuron. **c** The model of shunting inhibition for the CO<sub>2</sub> avoiding circuit in the *Drosophila* brain proposed in (Lin et al. 2013b). **d** PN<sub>v</sub>-1-like in **a** (green) and PN<sub>v</sub>-3-like in **b** (brown) and their top six putative downstream neurons (yellow) (i-vi)



Abundant irreducible loops were observed in the *Drosophila* brain network, whereas very few were observed in the random networks. While most of the strongest loops were found locally in the unilateral or bilateral ALs, loops that covered wide areas in the brain were also observed. Concerning the intra-community loops, the olfactory community dominated the short loops, and the longer loops were found to be mainly contributed by the motor community. The abundance of irreducible loops of the olfactory and motor communities might be related to the longer path length observed in these communities since there were fewer shortcuts. Short loops might be related to the recurrent and reverberatory propagation of the information (Wu et al. 2011; Krashes et al. 2007; Shih et al. 2015) as well as to the rhythmically synchronous firing activity (Mi et al. 2013). Interestingly, synchronous firing patterns have been observed in rodent olfactory bulbs (Cleland and Linster 2005; Kashiwadani et al. 1999), a homologous structure of insect AL. Longer loops are

potentially involved in multi-stage computation, which may be required by complex motor responses carried out in the motor community.

The statistical analysis presented here can be improved and extended in several ways. First, the true positive rate of the connection estimation is 40%, which means that the neural network we constructed is partial. The issue limits the power of analyses presented in this paper. The true positive rate can be further improved by new statistical tools and image registration methods, which will be developed in the future studies. Second, we did not consider the neuron types, or the putative neurotransmitters, in the present study. By distinguishing neuron types in the follow-up studies, we can perform more detailed analyses on the network and might be able to provide better interpretations to the unique network characteristics described in this study.

In conclusion, our mathematical analysis of the microscopic network of the *Drosophila* brain reveals that its structural

modularity highly correlates with functions. Moreover, we discovered strong diversity in terms of network architecture across communities. Such detailed structural diversity can only be observed in the microscopic network. Our study provides information that may help with the assessment of putative functions of the individual neurons and offers insights into the functional organisation of the *Drosophila* brain network.

## Information Sharing Statement

The neuronal data analysed in this work, including the images, reconstructed skeletons, predicted polarity and the derived network connectivity, are available at <http://flycircuit.tw> upon the publication of this paper.

**Acknowledgements** This work was supported by the Aim for the Top University Project of the Ministry of Education, and by the Higher Education Sprout Project funded by the Ministry of Science and Technology and Ministry of Education in Taiwan.

**Author Contributions** CTS, CCL, and ASC designed the study. CTS, YJL, CTW, TYW, CCC, and TSS performed the analysis. CTS and CCL wrote the manuscript. ASC provided the data.

## Compliance with Ethical Standards

**Competing Interests** The author(s) declare no competing interests.

## References

- Albert, R., & Barabasi, A. L. (2002). Statistical mechanics of complex networks. *Reviews of Modern Physics*, 74(1), 47–97.
- Azevedo, F. A. C., Carvalho, L. R. B., Grinberg, L. T., Farfel, J. M., Ferretti, R. E. L., Leite, R. E. P., et al. (2009). Equal numbers of neuronal and nonneuronal cells make the human brain an isometrically scaled-up primate brain. *The Journal of Comparative Neurology*, 513, 532–541. <https://doi.org/10.1002/cne.21974>.
- Bahlmann, K., So, P. T., Kirber, M., Reich, R., Kosicki, B., McGonagle, W., & Bellve, K. (2007). Multifocal multiphoton microscopy (MMM) at a frame rate beyond 600 Hz. *Optics Express*, 15, 10991–10998.
- Barrat, A., Barthelemy, M., Pastor-Satorras, R., & Vespignani, A. (2004). The architecture of complex weighted networks. *Proceedings of the National Academy of Sciences of the United States of America*, 101(11), 3747–3752. <https://doi.org/10.1073/pnas.0400087101>.
- Bassett, D. S., & Bullmore, E. (2006). Small-world brain networks. *Neuroscientist*, 12(6), 512–523. <https://doi.org/10.1177/1073858406293182>.
- Bewersdorf, J., Pick, R., & Hell, S. W. (1998). Multifocal multiphoton microscopy. *Optics Letters*, 23, 655–657.
- Bota, M., Dong, H. W., & Swanson, L. W. (2003). From gene networks to brain networks. *Nature Neuroscience*, 6(8), 795–799. <https://doi.org/10.1038/nn1096>.
- Bota, M., Sporns, O., & Swanson, L. W. (2015). Architecture of the cerebral cortical association connectome underlying cognition. *Proceedings of the National Academy of Sciences of the United States of America*, 112(16), E2093–E2101. <https://doi.org/10.1073/pnas.1504394112>.
- Brandes, U. (2001). A faster algorithm for betweenness centrality. *Journal of Mathematical Sociology*, 25(2), 163–177.
- Brin, S., & Page, L. (1998). *The anatomy of a large-scale hypertextual web search engine*. Paper presented at the seventh international world-wide web conference, Brisbane, Australia.
- Bullmore, E., & Sporns, O. (2009). *Complex brain networks: Graph theoretical analysis of structural and functional systems* [Research Support, N.I.H., Extramural research support, Non-U.S. Gov't. Review]. *Nature Reviews Neuroscience*, 10(3), 186–198. <https://doi.org/10.1038/nrn2575>.
- Chiang, A. S., Lin, C. Y., Chuang, C. C., Chang, H. M., Hsieh, C. H., Yeh, C. W., Shih, C. T., Wu, J. J., Wang, G. T., Chen, Y. C., Wu C. C., Chen, G. Y., Ching, Y. T., Lee, P. C., Lin, C. Y., Lin, H. H., Wu, C. C., Hsu, H. W., Huang, Y. A., Chen, J. Y., Chiang, H. J., Lu, C. F., Ni, R. F., Yeh, C. Y., & Hwang, J. K. (2011). Three-dimensional reconstruction of brain-wide wiring networks in *Drosophila* at single-cell resolution. [Research Support, Non-U.S. Gov't]. *Current Biology*, 21(1), 1–11. <https://doi.org/10.1016/j.cub.2010.11.056>.
- Cleland, T. A., & Linster, C. (2005). Computation in the olfactory system. *Chemical Senses*, 30, 801–813. <https://doi.org/10.1093/chemse/bji072>.
- Denk, W., & Horstmann, H. (2004). Serial block-face scanning electron microscopy to reconstruct three-dimensional tissue nanostructure. *PLOS Biology*, 2, e329. <https://doi.org/10.1371/journal.pbio.0020329>.
- Fagiolo, G. (2007). Clustering in complex directed networks. *Physical Review E*, 76(2), 026107.
- Fornito, A., Zalesky, A., & Bullmore, E. (2016). *Fundamentals of brain network analysis* (1st ed.). San Diego: Academic.
- Gămănuț, R., Kennedy, H., Toroczkai, Z., Ercsey-Ravasz, M., Van Essen, D. C., Knoblauch, K., et al. (2018). The mouse cortical connectome, characterized by an ultra-dense cortical graph, maintains specificity by distinct connectivity profiles. *Neuron*, 97(3), 698–715.e610. <https://doi.org/10.1016/j.neuron.2017.12.037>.
- Guimera, R., & Amaral, L. A. N. (2005). Functional cartography of complex metabolic networks. *Nature*, 433(7028), 895–900.
- Harriger, L., van den Heuvel, M. P., & Sporns, O. (2012). Rich club organization of macaque cerebral cortex and its role in network communication. *PLoS One*, 7(9), e46497. <https://doi.org/10.1371/journal.pone.0046497>.
- Helmstaedter, M. (2013). Cellular-resolution connectomics: Challenges of dense neural circuit reconstruction. *Nature Methods*, 10, 501–507. <https://doi.org/10.1038/nmeth.2476>.
- Hilgetag, C. C., & Goulas, A. (2016). Is the brain really a small-world network? *Brain Structure and Function*, 221(4), 2361–2366. <https://doi.org/10.1007/s00429-015-1035-6>.
- Homberg, U. (2008). Evolution of the central complex in the arthropod brain with respect to the visual system. *Arthropod Structure and Development*, 37(5), 347–362. <https://doi.org/10.1016/j.asd.2008.01.008>.
- Huang, Y.-C., Wang, C.-T., Su, T.-S., Kao, K.-W., Lin, Y.-J., Chuang, C.-C., et al. (2019). A single-cell level and connectome-derived computational model of the *Drosophila* brain. *Frontiers in Neuroinformatics*, 12, 99. <https://doi.org/10.3389/fninf.2018.00099>.
- Huisken, J., Swoger, J., Bene, F. D., Wittbrodt, J., & Stelzer, E. H. K. (2004). Optical sectioning deep inside live embryos by selective plane illumination microscopy. *Science*, 305, 1007–1009. <https://doi.org/10.1126/science.1100035>.
- Jefferis, G. S. X. E., Marin, E. C., Stocker, R. F., & Luo, L. (2001). Target neuron prespecification in the olfactory map of *Drosophila*. *Nature*, 414, 204–208. <https://doi.org/10.1038/35102574>.
- Jorgenson, L. A., Newsome, W. T., Anderson, D. J., Bargmann, C. I., Brown, E. N., Deisseroth, K., et al. (2015). The BRAIN initiative:

- Developing technology to catalyse neuroscience discovery. *Philosophical Transactions: Biological Sciences*, 370, 20140164. <https://doi.org/10.1098/rstb.2014.0164>.
- Kaiser, M. (2015). Neuroanatomy: Connectome connects fly and mammalian brain networks. *Current Biology*, 25(10), R416–R418. <https://doi.org/10.1016/j.cub.2015.03.039>.
- Kaiser, M., & Hilgetag, C. C. (2004). Edge vulnerability in neural and metabolic networks. *Biological Cybernetics*, 90(5), 311–317. <https://doi.org/10.1007/s00422-004-0479-1>.
- Kashiwadani, H., Sasaki, Y. F., Uchida, N., & Mori, K. (1999). Synchronized oscillatory discharges of mitral/tufted cells with different molecular receptive ranges in the rabbit olfactory bulb. *Journal of Neurophysiology*, 82, 1786–1792.
- Knox, J. E., Harris, K. D., Graddis, N., Whitesell, J. D., Zeng, H., Harris, J. A., et al. (2018). High resolution data-driven model of the mouse connectome. *bioRxiv*. <https://doi.org/10.1101/293019>.
- Krashes, M. J., Keene, A. C., Leung, B., Armstrong, J. D., & Waddell, S. (2007). Sequential use of mushroom body neuron subsets during Drosophila odor memory processing. *Neuron*, 53(1), 103–115. <https://doi.org/10.1016/j.neuron.2006.11.021>.
- Landhuis, E. (2017). Neuroscience: Big brain, big data. *Nature*, 541, 559–561. <https://doi.org/10.1038/541559a>.
- Lee, P. C., Chuang, C. C., Chiang, A. S., & Ching, Y. T. (2012). High-throughput computer method for 3D neuronal structure reconstruction from the image stack of the Drosophila brain and its applications. *PLoS Comput Biol*, 8(9), e1002658. <https://doi.org/10.1371/journal.pcbi.1002658>.
- Lee, Y. H., Lin, Y. N., Chuang, C. C., & Lo, C. C. (2014). SPIN: A method of skeleton-based polarity identification for neurons. *Neuroinformatics*, 12(3), 487–507. <https://doi.org/10.1007/s12021-014-9225-6>.
- Levoy, M., Ng, R., Adams, A., Footer, M., & Horowitz, M. (2006) Light Field Microscopy (SIGGRAPH '06, ACM, New York), <https://doi.org/10.1145/1179352.1141976>.
- Lichtman, J. W., Livet, J., & Sanes, J. R. (2008). A technicolour approach to the connectome. *Nature Reviews Neuroscience*, 9, 417–422. <https://doi.org/10.1038/nrn2391>.
- Lin, C. Y., Chuang, C. C., Hua, T. E., Chen, C. C., Dickson, B. J., Greenspan, R. J., & Chiang, A. S. (2013a). A comprehensive wiring diagram of the protocerebral bridge for visual information processing in the Drosophila brain. *Cell Reports*, 3(5), 1739–1753. <https://doi.org/10.1016/j.celrep.2013.04.022>.
- Lin, H. H., Chu, L. A., Fu, T. F., Dickson, B. J., & Chiang, A. S. (2013b). Parallel neural pathways mediate CO<sub>2</sub> avoidance responses in Drosophila. *Science*, 340(6138), 1338–1341. <https://doi.org/10.1126/science.1236693>.
- Lin, Y.-N., Chang, P.-Y., Hsiao, P.-Y., & Lo, C.-C. (2014). Polarity-specific high-level information propagation in neural networks. *Frontiers in Neuroinformatics*, 8, 27. <https://doi.org/10.3389/fninf.2014.00027>.
- Lo, C.-C., & Chiang, A.-S. (2016). Toward whole-body connectomics. *Journal of Neuroscience*, 36, 11375–11383. <https://doi.org/10.1523/JNEUROSCI.2930-16.2016>.
- Markram, H. (2012). The human brain project. *Scientific American*, 306(6), 50–55.
- Mayerich, D., Abbott, L., & McCORMICK, B. (2008). Knife-edge scanning microscopy for imaging and reconstruction of three-dimensional anatomical structures of the mouse brain. *Journal of Microscopy*, 231, 134–143. <https://doi.org/10.1111/j.1365-2818.2008.02024.x>.
- Mi, Y., Liao, X., Huang, X., Zhang, L., Gu, W., Hu, G., et al. (2013). Long-period rhythmic synchronous firing in a scale-free network. *Proceedings of the National Academy of Sciences*, 110, E4931–E4936. <https://doi.org/10.1073/pnas.1304680110>.
- Milo, R., Shen-Orr, S., Itzkovitz, S., Kashtan, N., Chklovskii, D., & Alon, U. (2002). Network motifs: Simple building blocks of complex networks. *Science*, 298(5594), 824–827. <https://doi.org/10.1126/science.298.5594.824>.
- Morgan, J. L., & Lichtman, J. W. (2013). Why not connectomics? *Nature Methods*, 10, 494–500. <https://doi.org/10.1038/nmeth.2480>.
- Muller, L., Destexhe, A., & Rudolph-Lilith, M. (2014). Brain networks: Small-worlds, after all? *New Journal of Physics*, 16(10), 105004. <https://doi.org/10.1088/1367-2630/16/10/105004>.
- Newman, M. E. J. (2006). Modularity and community structure in networks. *Proceedings of the National Academy of Sciences of the United States of America*, 103(23), 8577–8582. <https://doi.org/10.1073/pnas.0601602103>.
- Newman, M. E. J. (2010). *Networks: An introduction*. Oxford: Oxford University Press.
- Olsen, S. R., & Wilson, R. I. (2008). Lateral presynaptic inhibition mediates gain control in an olfactory circuit. *Nature*, 452, 956–960. <https://doi.org/10.1038/nature06864>.
- Pastrana, E. (2013). Focus on mapping the brain. *Nature Methods*, 10, 481–481. <https://doi.org/10.1038/nmeth.2509>.
- Peng, H., Ruan, Z., Long, F., Simpson, J. H., & Myers, E. W. (2010). V3D enables real-time 3D visualization and quantitative analysis of large-scale biological image data sets. *Nature Biotechnology*, 28(4), 348–353. <https://doi.org/10.1038/nbt.1612>.
- Planchon, T. A., Gao, L., Milkie, D. E., Davidson, M. W., Galbraith, J. A., Galbraith, C. G., & Betzig, E. (2011). Rapid three-dimensional isotropic imaging of living cells using Bessel beam plane illumination. *Nature Methods*, 8, 417–423. <https://doi.org/10.1038/nmeth.1586>.
- Plaza, S. M., Scheffer, L. K., & Chklovskii, D. B. (2014). Toward large-scale connectome reconstructions. *Current Opinion in Neurobiology*, 25, 201–210. <https://doi.org/10.1016/j.conb.2014.01.019>.
- Rubinov, M., & Sporns, O. (2010). Complex network measures of brain connectivity: Uses and interpretations. *Neuroimage*, 52(3), 1059–1069. <https://doi.org/10.1016/j.neuroimage.2009.10.003>.
- Scannell, J. W., Blakemore, C., & Young, M. P. (1995). Analysis of connectivity in the cat cerebral cortex. *Journal of Neuroscience*, 15(2), 1463–1483. <https://doi.org/10.1523/JNEUROSCI.15-02-01463.1995>.
- Schneider-Mizell, C. M., Gerhard, S., Longair, M., Kazimiers, T., Li, F., Zwart, M. F., et al. (2016). Quantitative neuroanatomy for connectomics in Drosophila. *Elife*, 5. <https://doi.org/10.7554/eLife.12059>.
- Shih, C.-T., Sporns, O., Yuan, S.-L., Su, T.-S., Lin, Y.-J., Chuang, C.-C., Wang, T. Y., Lo, C. C., Greenspan, R. J., & Chiang, A. S. (2015). Connectomics-based analysis of information flow in the Drosophila brain. *Current Biology*, 25, 1249–1258. <https://doi.org/10.1016/j.cub.2015.03.021>.
- Sporns, O., NetLibrary 10th Shared Collection, & Perpetual eBook Collection. (2011). *Networks of the brain* (pp. 1 online resource (xi, 412 p., [418] p. of plates)). Cambridge, MA: MIT Press.
- Sporns, O., Tononi, G., & Kotter, R. (2007). The human connectome: A structural description of the human brain. *PLoS Computational Biology*, 1(4), e42. <https://doi.org/10.1371/journal.pcbi.0010042>.
- Stocker, R. F. (1994). The organization of the chemosensory system in *Drosophila melanogaster*: A review. *Cell and Tissue Research*, 275, 3–26. <https://doi.org/10.1007/BF00305372>.
- Su, T.-S., Lee, W.-J., Huang, Y.-C., Wang, C.-T., & Lo, C.-C. (2017). Coupled symmetric and asymmetric circuits underlying spatial orientation in fruit flies. *Nature Communications*, 8(1), 139–115. <https://doi.org/10.1038/s41467-017-00191-6>.
- Triphan, T., Poeck, B., Neuser, K., & Strauss, R. (2010). Visual targeting of motor actions in climbing Drosophila. *Current Biology*, 20(7), 663–668. <https://doi.org/10.1016/j.cub.2010.02.055>.
- Watts, D. J. (1999). *Small worlds: The dynamics of networks between order and randomness*. Princeton: Princeton University Press.

- Watts, D. J., & Strogatz, S. H. (1998). Collective dynamics of 'small-world' networks. *Nature*, 393(6684), 440–442. <https://doi.org/10.1038/30918>.
- Wessnitzer, J., & Webb, B. (2006). Multimodal sensory integration in insects—towards insect brain control architectures. *Bioinspiration & Biomimetics*, 1(3), 63–75. <https://doi.org/10.1088/1748-3182/1/3/001>.
- Wu, C. L., Shih, M. F., Lai, J. S., Yang, H. T., Turner, G. C., Chen, L., & Chiang, A. S. (2011). Heterotypic gap junctions between two neurons in the *Drosophila* brain are critical for memory. *Current Biology*, 21(10), 848–854. <https://doi.org/10.1016/j.cub.2011.02.041>.
- Xiao, H., & Peng, H. (2013). APP2: Automatic tracing of 3D neuron morphology based on hierarchical pruning of a gray-weighted image distance-tree. *Bioinformatics*, 29(11), 1448–1454. <https://doi.org/10.1093/bioinformatics/btt170>.
- Zingg, B., Hintiryan, H., Gou, L., Song, M. Y., Bay, M., Bienkowski, M. S., Foster, N. N., Yamashita, S., Bowman, I., Toga, A. W., & Dong, H. W. (2014). Neural networks of the mouse neocortex. *Cell*, 156(5), 1096–1111. <https://doi.org/10.1016/j.cell.2014.02.023>.

**Publisher's Note** Springer Nature remains neutral with regard to jurisdictional claims in published maps and institutional affiliations.